FASTER-THAN-NATURAL SPACECRAFT CIRCUMNAVIGATION VIA WAY POINTS

Trevor Bennett and Hanspeter Schaub

8th International Workshop on Satellite Constellations and Formation Flying

Delft, Nederland **June 8–10, 2015**

FASTER-THAN-NATURAL SPACECRAFT CIRCUMNAVIGATION VIA WAY POINTS

Trevor Bennett* **and Hanspeter Schaub†**

Circumnavigation relative motion is considered for application such as inspecting a space object for damage, or characterizing space debris before engaging a remediation operation. Faster-than-natural circumnavigation is a control method in which the deputy spacecraft is advanced ahead of the natural Keplerian relative motion. Proposed is a state transition matrix method of generating a discrete way point guidance solution for faster-than natural circumnavigation. The state transition matrix methodology is applied to both circular and elliptical chief orbits. For the circular chief case, natural relative trajectories are planar in nature. With the faster-than-natural circumnavigation, this work illustrates how the required relative trajectories become three-dimensional curves. This methodology allows for closed-form impulsive control solutions and the associated fuel cost. The proposed method is validate through numerical simulation.

INTRODUCTION

Circumnavigation orbits are useful for inspection type missions such as searching for meteorite or space debris damage, to engage in servicing missions, or even to perform the proposed electrostatic tugging and formations.[1] The limitation of these circumnavigation relative orbits is that the natural solutions require one orbit period to complete. Further, the natural solutions may not provide the way points needed by the deputy satellite to get a good view of the chief satellite. This study utilizes the state transition matrix formulation to perform faster-than-natural circumnavigation via a set of pre-defined way-points. Several authors have explored the faster-than-natural relative orbits providing initial insight into continuous thrusting solutions. Reference 2 investigates using a bi-elliptic method to find a 2-impulse sequence to join 2 natural elliptic relative motions, yielding a faster-than-natural circumnavigation. Straight uses the relative motion State Transition Matrix (STM) for the circular chief case to develop impulsive control solutions to yield a non-natural circular circumnavigation solution.[3] Here a general set of way-points can be applied, and the STM is used to determine the the required changes in velocity at each way-point. Reference 4 also uses the circular chief STM to investigate using a series of way-points to perform a faster-than-natural approach to another space object. STM methods that scale to elliptic orbits are investigated in Reference 5. More recently, Dannemiller discusses the general STM approach to planning a multi-maneuver relative trajectory in Reference 6.

Faster-than-natural circumnavigation presents additional flexibility in the design of formation flying relative orbits. The STM-based approach provides opportunities for discrete guidance solutions

*Graduate Research Assistant, Aerospace Engineering Sciences, University of Colorado.
†Professor, Department of Aerospace Engineering Sciences, University of Colorado, 431 UCB, Colorado Center for Astrodynamics Research, Boulder, CO 80309-0431

with impulsive maneuvers. Consider two spacecraft in formation in the rotating local vertical local horizontal (LVLH) frame defined by Figure 1. Given the Keplerian orbits of the two spacecraft,

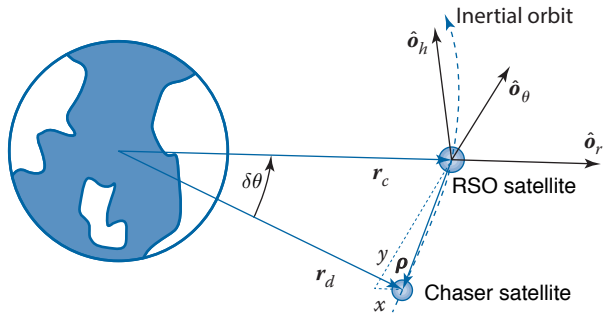

Figure 1. Local Vertical Local Horizontal rotating frame for formation flying.

the relative orbit of the deputy spacecraft remains constant and bounded. This paper investigates a method of advancing the deputy spacecraft to discrete points along the natural relative orbit in a faster time than otherwise feasible with the natural uncontrolled propagation of Keplerian motion. The concept of faster-than-natural circumnavigation is illustrated by the forced trajectory shown in Figure 2. The natural relative motion for the deputy spacecraft, under the assumption of Keplerian orbits, follows the dotted red trajectory around the chief spacecraft. Applying precise Δv maneuvers at way points, shown as blue points, enables the deputy spacecraft to reach the subsequent way point at a prescribed time denoted as t_i earlier than otherwise possible.

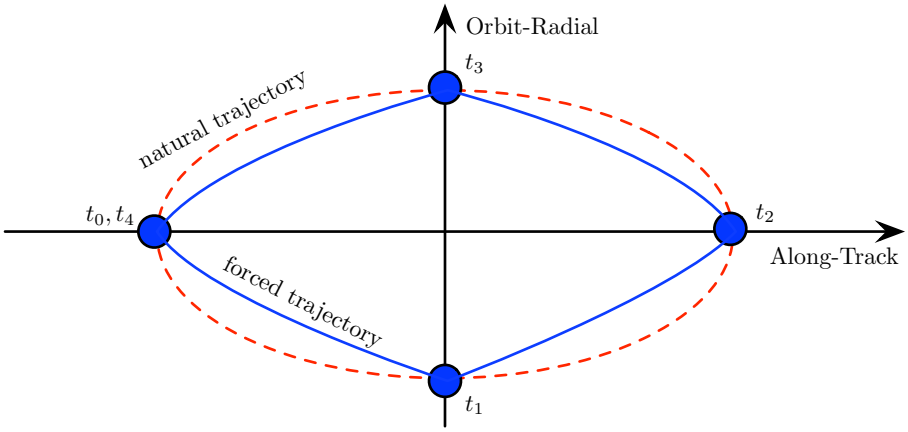

Figure 2. Illustration of Relative Motion Way Points

In this study the Keplerian relative motion STM is developed based on the orbit element difference approach. Alfriend and Gim develop the relative motion STM in Reference 7 assuming both point-mass and J_2 gravitational influences, even if eccentric chief motions are considered. In this paper, as control solutions implement non-natural relative trajectories, the impact of the J_2 perturbation is assumed to be minimal between two impulsive control burns. The simplified Gim/Alfriend STM is useful in developing analytical fuel consumption predictions, even for elliptic chief cases. Of interest is how does a non-natural relative orbit period impact the relative trajectory shape as the

circumnavigation time is sped up or down, while requiring the satellite still visit targeted way-points of naturally occurring relative trajectory. The naturally occurring relative orbits are planar, and the impact of changing the way-point visit time on the relative trajectory is investigated. Further, the approach scales to elliptic chief motions as well. While closed form solutions are feasible, their analytical expressions can be rather lengthly. The faster-than-natural way-point navigation is explored in simple 2 way-point scenario with a highly eccentric chief. The impact of the eccentric chief motion on the inter-way-point trajectories is investigated. Numerical simulations are used to demonstrate the resulting solutions.

CIRCUMNAVIGATION WAY POINTS

This study examines how a deputy spacecraft performs relative orbit maneuvers such that resulting circumnavigation is either faster or slower than the natural relative orbit period. The maneuver sequence is setup through a series of N_{wp} way points relative to the chief satellite as shown in Figure 2. The illustration shows a 2D in-plane relative trajectory. However, these way points can also contain out of plane z components. For simplicity in this study, even time segments are assumed between way points. If $P = \frac{2\pi}{n}$ is the natural relative motion period, then $T \leq P$ is the to circumnavigate through these way points. The time between way points is distributed evenly such that

$$T_i = \frac{T}{N_{\text{wp}}} \tag{1}$$

The time t_i for circular chief motion represents and intuitive geometrical division of the relative orbit. As is seen in later sections, equal segment time does not necessarily correspond to equal geometrical spacing. As desired, the deputy circumnavigation time will be less than the natural period and thus the speed up factor $0 < s < \infty$ is defined by

$$s = \frac{P}{T} \tag{2}$$

The speed up factor provides the natural motion for $s = 1$, slower than natural for $s < 1$, and faster than natural for $s > 1$. The sped up time between waypoints is expressed in terms of the chief mean orbital motion n and the number of way points N_{wp} as

$$T_i = \frac{2\pi}{nN_{\text{wp}}s} \tag{3}$$

As expected, increasing the speed up factor requires more ΔV. Also, the spacing of waypoints also impacts the ΔV budget. The influence from both the speed up and number of waypoints is addressed in later sections.

The following section presents the circular chief state transition matrix (STM) for the deputy spacecraft between way point maneuvers. Utilizing ΔV_i maneuvers between STM coast periods enables the faster than natural circumnavigation. The uniform spacing of the way points simplifies the following analysis, however the methodology is applicable to non-uniform way point spacing. The methodology is also expanded to an elliptical chief case presented in later sections.

RELATIVE MOTION STATE TRANSITION MATRIX

Desired is an analytic analysis of the waypoint propagation and ΔV budget given the prescrived relative orbit and speed up factor. The motion can be propagated through the use of a state transition

matrix that maps the current deputy position forward in time assuming Keplerian motion. Required is the relative position and velocity state of the deputy at the respective waypoints given the sequence of maneuvers. Let the relative motion state vector be

$$\boldsymbol{X} = \begin{bmatrix} x & y & z & \dot{x} & \dot{y} & \dot{z} \end{bmatrix}^T = \begin{bmatrix} \boldsymbol{r}^T & \boldsymbol{v}^T \end{bmatrix}^T \tag{4}$$

The state transition matrix $[\Phi_{\boldsymbol{X}}(t, t_0)]$ will map initial $\boldsymbol{X}(t_0) = \boldsymbol{X}_0$ states into the current states $\boldsymbol{X}(t)$ at time t through

$$\boldsymbol{X}(t) = [\Phi_{\boldsymbol{X}}(t, t_0)]\boldsymbol{X}_0 \tag{5}$$

An elegant solution to the STM is available using orbit elements. Consider the semi-non-singular orbit element set[8]

$$\boldsymbol{oe} = \{a, \theta, i, q_1, q_2, \Omega\} \tag{6}$$

where a is the semi-major axes, $\theta = \omega + f$ is the true latitude with the argument of periapse ω, true anomaly f , the inclination angle i. Defining $q_1 = e\cos\omega$ and $q_2 = e\sin\omega$ as measures of eccentricity e and argument of periapses with Ω as the ascending node angle completes the set.

In formation flying applications, the relative motion is small compared to the orbit radii and the linearized mapping $[A(\boldsymbol{oe}(t))]$ provides a convenient method to map orbit element differences into the Cartesian LVLH frame position and velocity counter parts.[8–10] The orbit element difference $\delta\boldsymbol{oe}(t)$ is obtained by differencing the deputy and chief orbit element sets with linearization about the chief element set.

$$\boldsymbol{X}(t) = [A(\boldsymbol{oe}(t))]\delta\boldsymbol{oe}(t) \tag{7a}$$

$$\boldsymbol{X}_0 = [A(\boldsymbol{oe}(t_0))]\delta\boldsymbol{oe}_0 \tag{7b}$$

The orbit element description has the benefit that assuming Keplerian motion all elements are constant, except for the anomaly measure (θ in the given $\boldsymbol{oe}$ set). Using the linearized mapping in Eq. (7), the state transition matrix $[\Phi_{\boldsymbol{X}}]$ can be found using:

$$[\Phi_{\boldsymbol{X}}(t, t_0)] = [A(\boldsymbol{oe}(t))][\Phi_{\delta\boldsymbol{oe}}(t, t_0)][A(\boldsymbol{oe}(t_0))]^{-1} \tag{8}$$

The matrix $[A(\boldsymbol{oe}(t))]$ is defined in parts by [8, p. 689-690]

$$[A(\boldsymbol{oe}(t))] = \begin{bmatrix} A_{11} & A_{12} \\ A_{21} & A_{22} \end{bmatrix} \tag{9a}$$

$$[A_{11}] = \begin{bmatrix} R/a & V_R R/V_T & 0 \\ 0 & R & 0 \\ 0 & 0 & R\mathrm{s}\theta \end{bmatrix} \tag{9b}$$

$$[A_{12}] = \begin{bmatrix} -R(2aq_1 + R\mathrm{c}\theta)/p & -R(2aq_2 + R\mathrm{s}\theta)/p & 0 \\ 0 & 0 & R\mathrm{c}i \\ 0 & 0 & -R\mathrm{c}\theta\mathrm{s}i \end{bmatrix} \tag{9c}$$

$$[A_{21}] = \begin{bmatrix} -V_R/(2a) & (1/R - 1/p)h & 0 \\ -3V_T/(2a) & -V_R & 0 \\ 0 & 0 & V_T\mathrm{c}\theta + V_R\mathrm{s}\theta \end{bmatrix} \tag{9d}$$

$$[A_{22}] = \begin{bmatrix} (V_R a q_1 + h\mathrm{s}\theta)/p & (V_R a q_2 - h\mathrm{c}\theta)/p & 0 \\ (3V_T a q_1 + 2h\mathrm{c}\theta)/p & (3V_T a q_2 + 2h\mathrm{s}\theta)/p & V_R\mathrm{c}i \\ 0 & 0 & (V_T\mathrm{s}\theta - V_R\mathrm{c}\theta)\mathrm{s}i \end{bmatrix} \tag{9e}$$

where the short-hand notation $\mathrm{c}\theta = \cos\theta$ and $\mathrm{s}\theta = \sin\theta$ is used, along with the definitions

$$R = r = \frac{a(1-q_1^2-q_2^2)}{1+q_1\mathrm{c}\theta+q_2\mathrm{s}\theta} \tag{10a}$$

$$V_R = \frac{h}{p}(q_1\mathrm{s}\theta - q_2\mathrm{c}\theta) \tag{10b}$$

$$V_T = \frac{h}{p}(1+q_1\mathrm{c}\theta+q_2\mathrm{s}\theta) \tag{10c}$$

$$p = a(1-e^2) \tag{10d}$$

$$h = \sqrt{\mu p} \tag{10e}$$

Here the orbit has semi-major axis a and eccentricity e about the central body with gravitational parameter μ . The inverse of $[A(\boldsymbol{oe}(t))]$ is taken to obtain $[A(\boldsymbol{oe}(t))]^{-1}$ with analytic solution in Reference 10.

The orbit element description has the benefit of assuming Keplerian motion with all elements are constant except for the anomaly measure (θ in the given $\boldsymbol{oe}$ set). Thus, the state transition matrix for the differential orbit elements $\delta\boldsymbol{oe}$ assumes the simple form [8, p. 697]

$$[\Phi_{\delta\boldsymbol{oe}}(t,t_0)] = \begin{bmatrix} 1 & 0 & 0 & 0 & 0 & 0 \\ A & B & 0 & C_1 & C_2 & 0 \\ 0 & 0 & 1 & 0 & 0 & 0 \\ 0 & 0 & 0 & 1 & 0 & 0 \\ 0 & 0 & 0 & 0 & 1 & 0 \\ 0 & 0 & 0 & 0 & 0 & 1 \end{bmatrix} \tag{11}$$

where

$$A = -\frac{3}{2}\frac{a\eta}{r^2}nt \tag{12a}$$

$$B = \left(\frac{r_0}{r}\right)^2 \tag{12b}$$

$$\begin{aligned} C_1 = \frac{1}{r^2\eta^2}\Big(&r\mathrm{s}\theta(r+a(1-q_1^2)) - r_0\mathrm{s}\theta_0(r_0+a(1-q_1^2)) + aq_1q_2(r\mathrm{c}\theta - r_0\mathrm{c}\theta_0) \\ &+ q_2(r-r_0)(a+r+r_0)\Big) \end{aligned} \tag{12c}$$

$$\begin{aligned} C_2 = \frac{1}{r^2\eta^2}\Big(&-r\mathrm{c}\theta(r+a(1-q_2^2)) + r_0\mathrm{c}\theta_0(r_0+a(1-q_2^2)) - aq_1q_2(r\mathrm{s}\theta - r_0\mathrm{s}\theta_0) \\ &- q_1(r-r_0)(a+r+r_0)\Big) \end{aligned} \tag{12d}$$

using the following definitions in terms of $\boldsymbol{oe}$:

$$\eta = \sqrt{1-q_1^2-q_2^2} \tag{13}$$

$$r = \frac{a\eta^2}{1+q_1\cos\theta+q_2\sin\theta} \tag{14}$$

$$r_0 = \frac{a\eta^2}{1+q_1\cos\theta_0+q_2\sin\theta_0} \tag{15}$$

Note that this solution to $[\Phi_{\delta\boldsymbol{\alpha e}}]$ assumes that $\theta(t)$ is found separately by solving Kepler's equation. For circular chief motion, the implementation of Kepler's equation reduces simply such that the change in time is the change in angle by mean motion. The more complicated inclusion of time of flight is discussed in the specific derivation of the elliptical chief motion. Therefore, the state transition matrix $[\Phi_{\boldsymbol{X}}]$ can be found using

$$[\Phi_{\boldsymbol{X}}(t,t_0)] = [A(t)][\Phi_{\delta\boldsymbol{\alpha e}}(t,t_0)][A(t_0)]^{-1} \tag{16}$$

Using the linearized mapping in Eq. (7) and extensive algebraic simplification of Eq. (8) provides the state transition matrix for general spacecraft motion. This methodology applies generally to Keplerian linearized relative motion. The only restriction to the presented methodology is that the inclination angle must be non-zero, $i \neq 0$. However, this constraint is irrelevant for circular chief relative motion and the planar relative motion discussed in the elliptical chief development.

Provided the analytic form of the state transition matrix, we can solve for the next waypoint position $\boldsymbol{r}_{i+1}$ in terms of the current waypoint position $\boldsymbol{r}_i$ and the corresponding departure velocity $\boldsymbol{v}_i^+$ using impulsive burns.

$$\boldsymbol{r}_{i+1} = [\Phi_{\boldsymbol{X},11}(t_{i+1},t_i)]\boldsymbol{r}_i + [\Phi_{\boldsymbol{X},12}(t_{i+1},t_i)]\boldsymbol{v}_i^+ \tag{17}$$

Given the $\boldsymbol{r}_i$ and $\boldsymbol{r}_{i+1}$ waypoint information, this can be solved for the current waypoint desired open-loop departure velocity $\boldsymbol{v}_i^+$ using

$$\boldsymbol{v}_i^+ = [\Phi_{\boldsymbol{X},12}(t_{i+1},t_i)]^{-1}\left(\boldsymbol{r}_{i+1} - [\Phi_{\boldsymbol{X},11}(t_{i+1},t_i)]\boldsymbol{r}_i\right) \tag{18}$$

where $[\Phi_{\boldsymbol{X},12}(t_{i+1},t_i)]^{-1}$ maps the position error back to the present state. Applying the impulsive burn, the expected arrival velocity at the next way point is given by

$$\boldsymbol{v}_{i+1}^- = [\Phi_{\boldsymbol{X},21}(t_{i+1},t_i)]\boldsymbol{r}_i + [\Phi_{\boldsymbol{X},22}(t_{i+1},t_i)]\boldsymbol{v}_i^+ \tag{19}$$

Thus, the open-loop burn $\Delta\boldsymbol{v}_i$ at the i^{th} way point is given by

$$\Delta\boldsymbol{v}_i = \boldsymbol{v}_i^+ - \boldsymbol{v}_i^- \tag{20}$$

with the total ΔV budget as the sum of all waypoint burns. Considered in the following sections are three implementations of the proposed methodology. First presented is the circular chief case with both 4 and 2 waypoint solutions. Following is the elliptic chief case results using two waypoints.

CIRCULAR CHIEF CIRCUMNAVIGATION

Of interest are relative orbits around a circular chief. Significant simplification of Eq. (8) is possible using $r \to a$, $r_0 \to a$, and with zero eccentricity $q_1 \to 0$, and $q_2 \to 0$. The resulting STM

for linearized motion around a circular chief is[11]

$$[\Phi_{\boldsymbol{X}}] = \begin{bmatrix} \Phi_{\boldsymbol{X},11} & \Phi_{\boldsymbol{X},12} \\ \Phi_{\boldsymbol{X},21} & \Phi_{\boldsymbol{X},22} \end{bmatrix} \tag{21a}$$

$$[\Phi_{\boldsymbol{X},11}] = \begin{bmatrix} 4-3\cos(nt) & 0 & 0 \\ 6(\sin(nt)-nt) & 1 & 0 \\ 0 & 0 & \cos(nt) \end{bmatrix} \tag{21b}$$

$$[\Phi_{\boldsymbol{X},12}] = \begin{bmatrix} \frac{\sin(nt)}{n} & \frac{2(1-\cos(nt))}{n} & 0 \\ -\frac{2(1-\cos(nt))}{n} & \frac{4\sin(nt)}{n} - 3t & 0 \\ 0 & 0 & \frac{\sin(nt)}{n} \end{bmatrix} \tag{21c}$$

$$[\Phi_{\boldsymbol{X},21}] = \begin{bmatrix} 3n\sin(nt) & 0 & 0 \\ -6n(1-\cos(nt)) & 0 & 0 \\ 0 & 0 & -n\sin(nt) \end{bmatrix} \tag{21d}$$

$$[\Phi_{\boldsymbol{X},22}] = \begin{bmatrix} \cos(nt) & 2\sin(nt) & 0 \\ -2\sin(nt) & 4\cos(nt)-3 & 0 \\ 0 & 0 & \cos(nt) \end{bmatrix} \tag{21e}$$

Recall that in the circular chief case, the change in anomaly angle is $\Delta f = \Delta M = nt$. The change in angle is easily obtained from Kepler's equation for any point-to-point state transition in a circular orbit. Therefore the simplification $\Delta f = nt = \alpha$ is employed enabling any point-to-point transition. The constant $[\Phi_{\boldsymbol{X},ij}]$ state transition sub-matrices are then simplified to

$$[\Phi_{\boldsymbol{X},11}] = \begin{bmatrix} 4-3\cos(\alpha) & 0 & 0 \\ 6(\sin(\alpha)-\alpha) & 1 & 0 \\ 0 & 0 & \cos(\alpha) \end{bmatrix} \tag{22a}$$

$$[\Phi_{\boldsymbol{X},12}] = \begin{bmatrix} \frac{\sin(\alpha)}{n} & \frac{2(1-\cos(\alpha))}{n} & 0 \\ -\frac{2(1-\cos(\alpha))}{n} & \frac{4\sin(\alpha)}{n} - \frac{3\alpha}{n} & 0 \\ 0 & 0 & \frac{\sin(\alpha)}{n} \end{bmatrix} \tag{22b}$$

$$[\Phi_{\boldsymbol{X},21}] = \begin{bmatrix} 3n\sin(\alpha) & 0 & 0 \\ -6n(1-\cos(\alpha)) & 0 & 0 \\ 0 & 0 & -n\sin(\alpha) \end{bmatrix} \tag{22c}$$

$$[\Phi_{\boldsymbol{X},22}] = \begin{bmatrix} \cos(\alpha) & 2\sin(\alpha) & 0 \\ -2\sin(\alpha) & 4\cos(\alpha)-3 & 0 \\ 0 & 0 & \cos(\alpha) \end{bmatrix} \tag{22d}$$

The following algorithm makes use of the inverse of $[\Phi_{\boldsymbol{X},12}]$. The analytical inverse solution is given as

$$[\Phi_{\boldsymbol{X},12}]^{-1} = \frac{1}{\kappa} \begin{bmatrix} n(3\alpha - 4\sin\alpha) & 2n(1-\cos\alpha) & 0 \\ -2n(1-\cos\alpha) & -n\sin\alpha & 0 \\ 0 & 0 & \kappa n \csc\alpha \end{bmatrix} \tag{23}$$

with

$$\kappa = 8\cos\alpha + 3\alpha\sin\alpha - 8 \tag{24}$$

The analytic form for the open loop Δv enables fuel and time cost analysis and enables parameter tuning. Visualization of these results is presented in the following sections.

SIMULATED 4 WAYPOINT STUDY

Simulation of the open-loop Δv computation provides visualization of the faster-than-natural circumnavigation concept. Consider the circular chief case where $N_{\text{wp}} = 4$ with $A_0 > 0$ and $B_0 > 0$. In the current study the waypoints are assumed to have even temporal spacing throughout the maneuver. The maneuver time T_i between waypoints is given in Eq. (3). Assuming a general number N_{wp} of waypoints leads to

$$t = T_i = \frac{1}{n} \underbrace{\frac{2\pi}{N_{\text{wp}} s}}_{\alpha} = \frac{\alpha}{n} \tag{25}$$

For the specific case where $N_{\text{wp}} = 4$, then

$$\alpha = \frac{\pi}{2s} \tag{26}$$

The motion between the waypoints is computed using the STM mapping

$$\boldsymbol{X}(t) = [\Phi_{\boldsymbol{X}}(t, t_i)]\boldsymbol{X}(t_i) \qquad \forall\, t_i < t < t_{i+1} \tag{27}$$

The faster than natural circumnavigation study focuses on the open-loop impulsive burns where Eq. (5) is also used to generate the reference motion. The presented form in Eq. (27) allows for any reference motion to be prescribed from any set of initial relative orbit conditions. This form is also employed in the elliptic chief case.

A variety of relative orbits are available for study. Considered here is a generic 2-1 planar ellipse with an equivalent radial and normal component magnitude. The mean motion of the chief is fixed at $n = 0.0007$ rad/s. The considered 4 waypoint positions are given in sequence by

$$\boldsymbol{r}(t_0) = -2A_0\hat{\boldsymbol{o}}_\theta \tag{28a}$$
$$\boldsymbol{r}(t_1) = -A_0\hat{\boldsymbol{o}}_r - B_0\hat{\boldsymbol{o}}_h \tag{28b}$$
$$\boldsymbol{r}(t_2) = +2A_0\hat{\boldsymbol{o}}_\theta \tag{28c}$$
$$\boldsymbol{r}(t_3) = A_0\hat{\boldsymbol{o}}_r + B_0\hat{\boldsymbol{o}}_h \tag{28d}$$
$$\boldsymbol{r}(t_4) = -2A_0\hat{\boldsymbol{o}}_\theta \tag{28e}$$

The prescribed points reside on the nominal trajectory. Enforced are the endpoint velocities to start from and end on the nominal relative orbit.

$$\boldsymbol{v}(t_0^-) = \boldsymbol{v}(t_0^+) = -nA_0\hat{\boldsymbol{o}}_r - nB_0\hat{\boldsymbol{o}}_h \tag{29}$$

The "-" super-script indicates the Hill frame velocity prior to a burn, and the "+" super-script indicates the post-burn Hill frame velocity.

Provided an analytical expression for the STM in Eq. (22), desired is the total ΔV required to perform a particular faster-than-natural circumnavigation. To simplify the following descriptions, the two parameter definitions are introduced

$$\beta_1 = 1 - \sin\alpha - \cos\alpha \tag{30a}$$
$$\beta_2 = 1 + \sin\alpha - \cos\alpha \tag{30b}$$

Time	$\Delta \boldsymbol{v}_i \cdot \hat{\boldsymbol{o}}_r$	$\Delta \boldsymbol{v}_i \cdot \hat{\boldsymbol{o}}_\theta$	$\Delta \boldsymbol{v}_i \cdot \hat{\boldsymbol{o}}_h$
t_0	$\frac{A_0 n}{\kappa}(3\alpha \sin(\alpha) - 3\alpha - 4\beta_1)$	$\frac{2A_0 n \beta_1}{\kappa}$	$-B_0 n \csc \alpha$
t_1	$\frac{2A_0 n}{\kappa}(4\beta_1 + 3\alpha \cos \alpha)$	0	$2B_0 n \cot \alpha$
t_2	0	$-\frac{4A_0 n \beta_1}{\kappa}$	0
t_3	$-\frac{2A_0 n}{\kappa}(4\beta_1 + 3\alpha \cos \alpha)$	0	$-2B_0 n \cot \alpha$
t_4	$\frac{A_0 n}{\kappa}(3\alpha \sin(\alpha) - 3\alpha - 4\beta_1)$	$\frac{2A_0 n \beta_1}{\kappa}$	$B_0 n \csc \alpha$

Table 1. Analytical Δv_i Burn Solution for a 4-Waypoint Circumnavigation Maneuver

The analytical prediction for the 4 way-point ΔV utilizes the definition in Eq. (20). The analytic ΔV requirement at each way-point is tabulated in Table for the prescribed waypoint sequence in Eq. (28). To evaluate the total fuel cost, the $\Delta \boldsymbol{v}_i$'s about each body axes are summed using

$$\Delta v_{\text{total}} = \sum_{i=0}^{N_{\text{wp}}} = |\Delta \boldsymbol{v}_i \cdot \hat{\boldsymbol{o}}_r| + |\Delta \boldsymbol{v}_i \cdot \hat{\boldsymbol{o}}_\theta| + |\Delta \boldsymbol{v}_i \cdot \hat{\boldsymbol{o}}_h| \tag{31}$$

Using the analytic form in Table , the total Δv simplifies to

$$\Delta v_{\text{total}} = \frac{2A_0 n}{|\kappa|}\left(4|\beta_1| + 2|4\beta_1 + 3\alpha \cos(\alpha)| + |3\alpha + 4\beta_1 - 3\alpha \sin(\alpha)|\right) + 2B_0 n\left(|\cot(\alpha)| + |1 - \csc(\alpha)|\right) \tag{32}$$

The particular multi-burn circumnavigation strategy is implemented in Mathematica. The speedup factor is set to $s = 1.7$ for faster-than-natural and $s = 0.75$ for slower-than natural. The relative orbit parameters are set to $A_0 = B_0 = 10$ meters. The resulting relative motion is illustrated in Figure 3 with nominal in grey. Figure 3 does not provide clear visualization of the inertial transfer orbits to hop between waypoints. However, it does provide significant insight into the warping of the relative motion required for faster than natural circumnavigation. The in-plane projection in Figure 3(a) shows that the sped up circumnavigation shown in red requires sharper trajectory changes at the waypoints on the along-track axis. The along-track view in Figure 3(b) shows that in order to meet the out-of-plane waypoints, the relative motion is not longer a planar curve, but rather a three-dimensional curve. The planar view in Figure 3(a) exhibits the expected squeeze in the relative motion plane. More interestingly, the along-track view in Figure 3(b) reveals the true warping. Presented is a speed up factor of $s = 1.7$ and $s = 0.75$. The slower than natural motion warps in the opposite manner to the faster than natural motion. The planar motion seen in Figure 3(a) shows that the relative motion expands with the local velocity at each waypoint driving the spacecraft out away from the nominal. The along-track view in Figure 3(b) shows how the spacecraft shifts largely out-of-plane to delay the arrival.

Sweeping through the speed up factors above unity reveals that the maximum warping of the along-track view occurs with $s = 2$. This is evidenced in Figure 4. The value $s = 2$ physically describes a series of transfer orbits that phase the deputy spacecraft by half a period. As expected

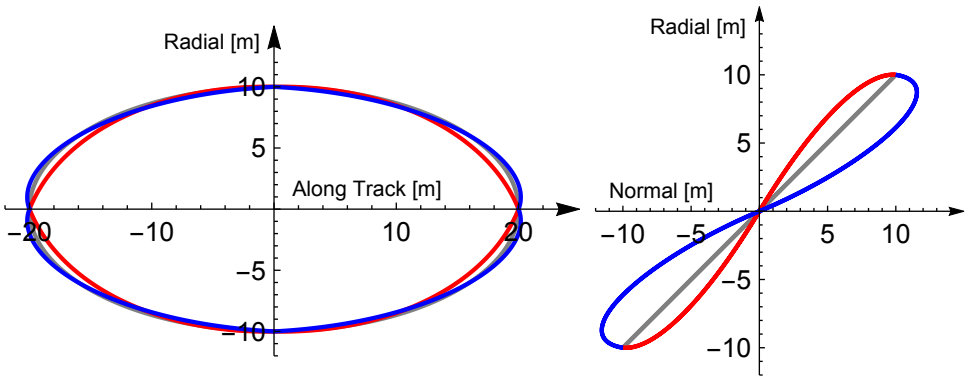

(a) In-Pane View (b) Along-Track View

Figure 3. Open-Loop Forced 4 Waypoint Circumnavigation Illustration using $A_0 = B_0 = 10$ meters. (— s = 1.7, — s = 0.75, — Natural Motion)

with the circular chief, the faster than natural relative motion is symmetric. This symmetry breaks down for the elliptic chief case. Increasing the speed up factor such that $s > 2$ transitions the relative orbit geometry towards hyperbolic point-to-point trajectories. This manifests an along-track view warping that decreases back into the nominal plane. The slower-than-natural solutions, $s < 1$, exhibit an exponential divergence from the nominal relative orbit as the new trajectory approaches the infinite size relative orbit at $s = 0$.

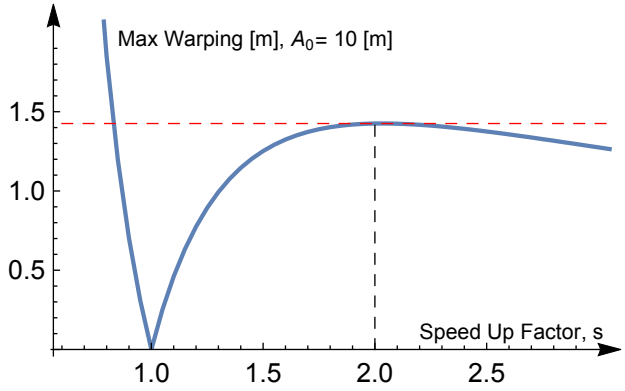

Figure 4. Maximum warping away from the nominal planar circumnavigation.

The decrease in speed up factor from unity introduces a greater sensitivity in geometry change and ΔV requirement than does the increase in speed up factor. This is evidenced in Figure 5 where variations in the speed up factor and relative orbit sizing are considered. The nominal $s = 1$ does not require any burns and is marked with the dashed red line. The asymmetry in speed up factor and the increased requirement for larger orbits are visible in Figure 5. Consistent with the more substantial relative orbit change seen in Figure 3 for the slower circumnavigation, Figure 5 highlights the more rapidly increasing ΔV requirement for the same increment of change in the speed up factor. Recall that the speed up factor appears in the denominator of the time of flight. It is therefore expected that decreasing s towards zero will have an inverse power increase in ΔV with an inverse power decrease towards larger speed up factors. Further exhibited is the increase in ΔV as the geometry

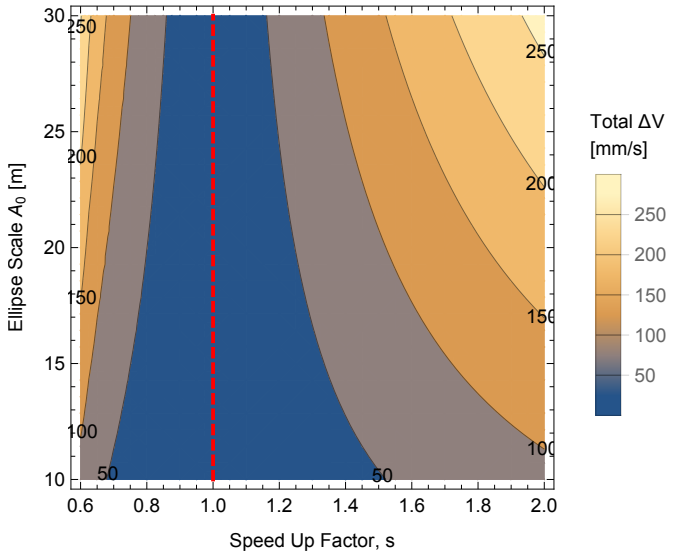

Figure 5. Total ΔV for the 4 waypoint circular chief. Nominal is shown by —- .

enlarges. This is as expected as greater distance reduction is required for larger geometries with the same speed up factor.

Presented is a circular chief faster than natural circumnavigation example. Given the trajectory magnitudes considered, Figure 5 demonstrates the speed up is feasible with less than 250 mm/s. The following sections introduce the elliptic chief case and another circular chief case used for comparison.

SIMULATED 2 WAYPOINT STUDY FOR COMPARISON

Desired is the more general form for faster-than-natural circumnavigation enabling implementations with an elliptic chief. As mentioned in the derivation of the state transition matrix form, the elliptic chief does not have a linear relationship between time of flight and true anomaly change. Therefore, the elliptic chief waypoints are set to periapse and apoapse for simplicity in the STM although the proposed methodology applies generally.

Consider first a comparison case where the chief is held circular and only the periapse and apoapse waypoints are used. Utilizing the decoupling, the out-of-plane motion is removed to provide isolation of the eccentric influence on planar relative motion. The mean motion of the chief is fixed at $n = 0.0007$ rad/s and the considered 2 waypoint positions are given in sequence by

$$\boldsymbol{r}(t_0) = -2A_0\hat{\boldsymbol{o}}_\theta \tag{33a}$$

$$\boldsymbol{r}(t_1) = +2A_0\hat{\boldsymbol{o}}_\theta \tag{33b}$$

$$\boldsymbol{r}(t_2) = \boldsymbol{r}(t_0) \tag{33c}$$

Again, enforced are the endpoint velocities to start from and end on the nominal relative orbit.

$$\boldsymbol{v}(t_0^-) = \boldsymbol{v}(t_0^+) = -nA_0\hat{\boldsymbol{o}}_r \tag{34}$$

Similar to the development employed in Table **??**, an analytic expression for the 2 way-point circular chief ΔV is available and is not included here. The prescribed nominal relative motion and

the relative orbits with a speed up factors of $s = 1.7$ and $s = 0.75$ are shown in Figure 6. Unlike the planar motion seen in Figure 3(a), the faster circumnavigation traverses outside of the nominal trajectory at the most radial nodes. The relaxation of the waypoints down from 4 to 2 moves the circumnavigation closer to the efficiency of a 2-burn phasing maneuver. The important feature in Figure 6 is that the relative motion remains symmetric for each segment with the circular chief.

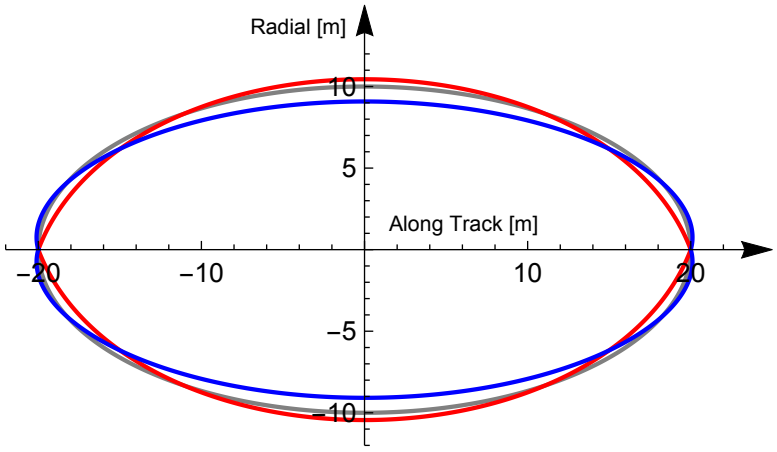

Figure 6. Open-Loop Forced 2 Waypoint Circumnavigation using $A_0 = 10$ and $B_0 = 0$ meters. (— s = 1.7, — s = 0.75, — Natural Motion)

The reduced ΔV requirements are characterized in Figure 7. The respective ΔV magnitudes have diminished in comparison to Figure 5. Comparison of Figure 5 and Figure 7 demonstrates the trend towards the more efficient 2-burn phasing solution.

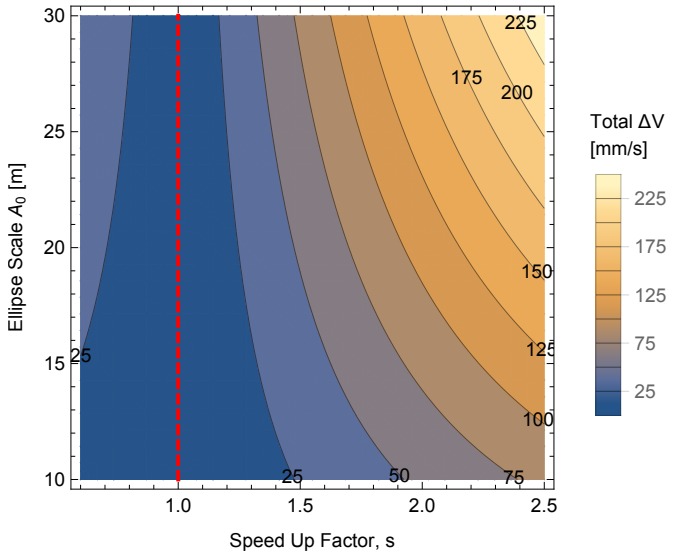

Figure 7. Total ΔV for the 2 waypoint circular chief. Nominal is shown by — .

The circular chief examples are fully presented with comparisons drawn between 2 and 4 waypoint solutions. The proposed faster than natural circumnavigation STM methodology is again ap-

plied to an elliptic chief. The results of the circular chief sections provide insight into the influence of ellipticity.

ELLIPTICAL CHIEF STM DEVELOPMENT

Desired is an elliptical chief faster than natural circumnavigation solution. The prescription of the relative orbit fundamentally changes in moving to an elliptic chief. Consider the conceptual visualization of the faster-than-natural circumnavigation with an elliptic chief shown in Figure 8. The nominal waypoints are placed at the periapse and apoapse locations with respective LVLH frames. The true anomaly for the nominal relative motion propagates from 0 to π for the first segment and π to 2π for the second segment. The faster-than-natural circumnavigation advances the relative orbit waypoints to an earlier true anomaly. The red LVLH frames shown in Figure 8 represent the new relative motion coordinate systems at the advanced true anomaly positions. Also seen in Figure 8 is the two part propagation through $\Delta f = \pi/s$ which is fundamental to the STM construction.

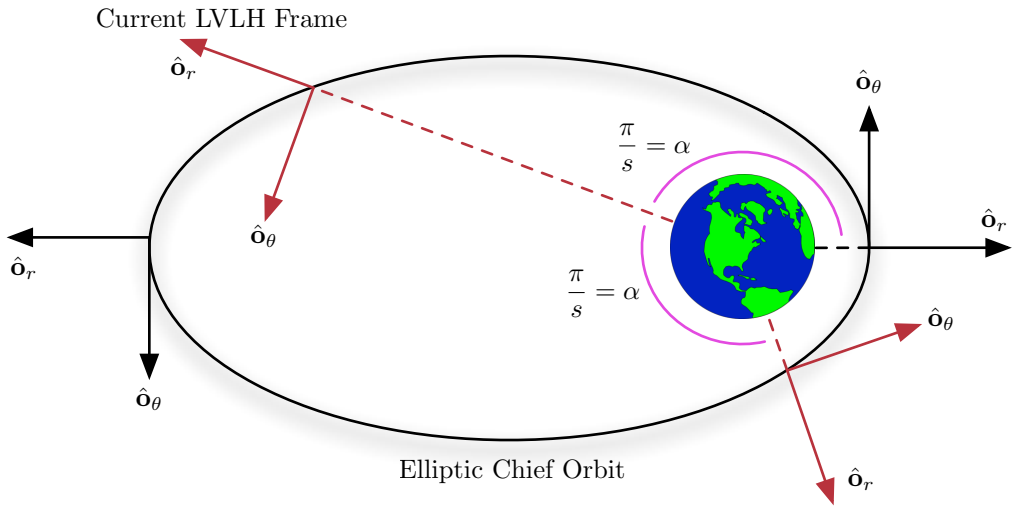

Figure 8. Speed up factor influence on the positions of the waypoints for the elliptic chief.

The required STMs are constructed from the Eq. (8). In the circular chief case, the time of flight and the change in anomaly angle were linearly related. In the eccentric chief, the time of flight and true anomaly change are not linearly related. Further, in Eq. (10) the gravitational parameter μ and the semi-major axis a appear in the STM. The equations can be non-dimensionalized by introducing the mean motion $n = \sqrt{\mu/a^3}$. The resulting elliptic chief STM retains terms of the form nt. The time of flight t can be removed from the STM by inserting the geometrical change provided by Kepler's equation. Recall, the time-of-flight for a spacecraft under 2-Body motion is expressed by Kepler's equation

$$M(t) = M_0 + n(t - t_0) \tag{35}$$

Given that the desired FTNC requires a mapping to the true anomaly speed-up, the definition of the eccentric anomaly from the mean anomaly is utilized

$$M(t) = E(t) - e\sin(E(t)) \tag{36}$$

Further, the eccentric anomaly is related to the true anomaly through

$$\tan\left(\frac{E(t)}{2}\right) = \sqrt{\frac{1-e}{1+e}}\tan\left(\frac{f(t)}{2}\right) \tag{37}$$

The time of flight $t - t_0$ is therefore obtained by inserting Eq. (36) into Eq. (35) with the definitions in Eq. (37). The use of Kepler's equation dictates that a general STM for all segments does not exist for the elliptic chief trajectory. That is, a unique STM is constructed for each segment. In the case of the two waypoint solution, the respective STMs employed are

$$[\Phi_{\boldsymbol{X},1}(f = \frac{\pi}{s}, f_0 = 0)] \qquad [\Phi_{\boldsymbol{X},2}(f = \frac{2\pi}{s}, f_0 = \frac{\pi}{s})] \tag{38}$$

The speed up factor is present in the elliptic STMs such that the midpoint maneuver happens at a shifted true anomaly. Effectively, the speed up factor advances the true anomaly of the relative orbit geometry. The second state transition matrix $[\Phi_{\boldsymbol{X},2}]$ may often span across the chief apoapse and introduces substantial relative motion influence for the later half of the trajectories considered.

For the following visualizations, the chief eccentricity is set to a modest $e = 0.3$ with a mean motion of $n = 0.0007$ rad/s. The argument of periapse is set to zero and the inclination of the chief orbit does not appear in the planar relative orbit case. The considered 2 waypoint positions are given in sequence by

$$\boldsymbol{r}(t_0) = -2A_0\hat{\boldsymbol{o}}_\theta \tag{39a}$$
$$\boldsymbol{r}(t_1) = [\Phi_{\boldsymbol{X},1}(f = \pi, f_0 = 0)]\boldsymbol{X}(t_0) \approx +2.2A_0\hat{\boldsymbol{o}}_\theta \tag{39b}$$
$$\boldsymbol{r}(t_2) = \boldsymbol{r}(t_0) \tag{39c}$$

The nominal velocity conditions enforced are the endpoint velocities.

$$\boldsymbol{v}(t_0^-) = \boldsymbol{v}(t_0^+) = -nA_0\hat{\boldsymbol{o}}_r \tag{40}$$

The prescribed nominal relative motion and the relative orbits with a speed up factor of $s = 1.7$ and speed of $s = 0.88$ are shown in Figure 9. The first segment of the faster than natural trajectory appears to have similar form to the segments seen in the circular chief. As anticipated, the second part of the relative motion segment experiences dramatically different character than the circular chief. Most notable is the turn inward well inside the near 2-1 nominal ellipse. Recall that the trajectory begins in a trailing along-track position and then transitions into the negative radial towards the leading along track position. A critical set of features in Figure 9 are the kinks in the relative motion trajectory. These kinks are indicative of apoapse and periapse crossings. Careful inspection of the first segment in the slower than natural trajectory reveals a kink at the largest along-track magnitude. Utilizing a speed up factor of $s = 0.88$ dictates that the first waypoint is reached after the chief has passed through apoapse. The trajectory kink marks the chief apoapse crossing. Observe the most clear kink in the second half of the slower than natural trajectory in Figure 9 where the trajectory nearly aligns with the nominal. The slowed trajectory reaches the second waypoint, or the original relative position, after the chief has passed periapse. The chief periapse crossing introduces this kink. Careful inspection reveals that a kink also exists in the faster than natural trajectory just following the second segment crossing a zero along-track position. This kink event marks the chief apoapse crossing for the faster than natural circumnavigation.

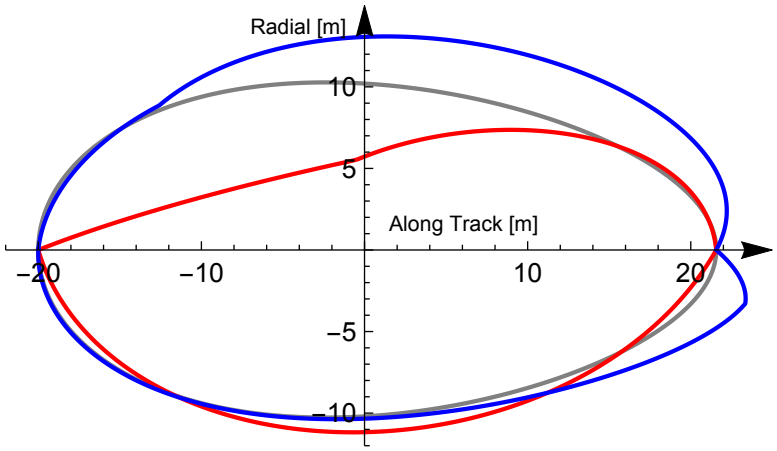

Figure 9. Open-Loop Forced 2 Waypoint Circumnavigation using $A_0 = 10$ meters. (— s = 1.7, — s = 0.88, — Natural Motion)

The effective of an elliptic chief is evidenced in the kinked relative motion trajectories for faster than natural circumnavigation. The behavior is further examined with a sweep of speed up factors ranging over $s_{\text{min}} = 1.1$ to $s_{\text{max}} = 1.9$ with an increment of $\Delta s = 0.2$. The collection of trajectories is displayed in sweeping color shown in Figure 10. Careful inspection of Figure 10 reveals the chief apoapse crossing in all trajectories. As expected, the larger the speed up the later in the second segment the kink appears.

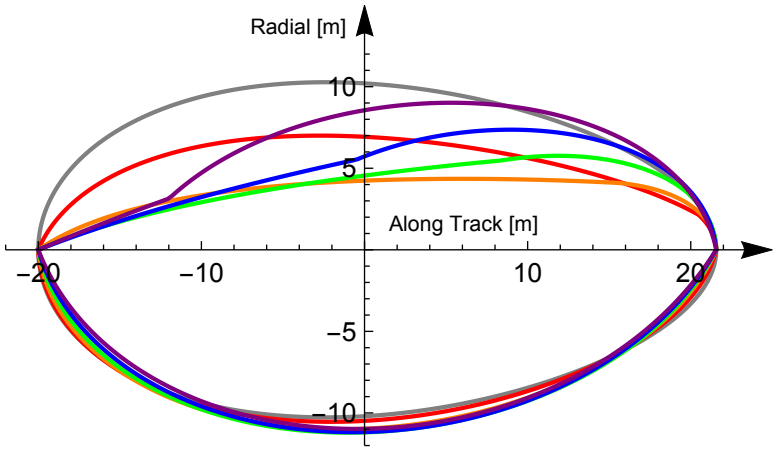

Figure 10. Open-Loop Forced 2 Waypoint Circumnavigation using $A_0 = 10$ and $B_0 = 0$ meters. (— s = 1.1, — s = 1.3, — s = 1.5, — s = 1.7, — s = 1.9, — Natural Motion)

The behavior in Figure 10 influences the ΔV requirement sweep with clear speed up markers. Figure 11 presents a sweep of the speed up factor and initial position geometry. Inspection of $s = 2$ in Figure 11 reveals a kink transition in the smooth contour. The physical significance of the $s = 2$ vertical is that speed up factors greater than 2 never cross the chief apoapse. An increasing negative slope is present immediately following the $s = 2$ vertical suggesting a discontinuity in efficiency

change for such transfers. Comparison of Figure 11 and the circular chief case in Figure 7 shows

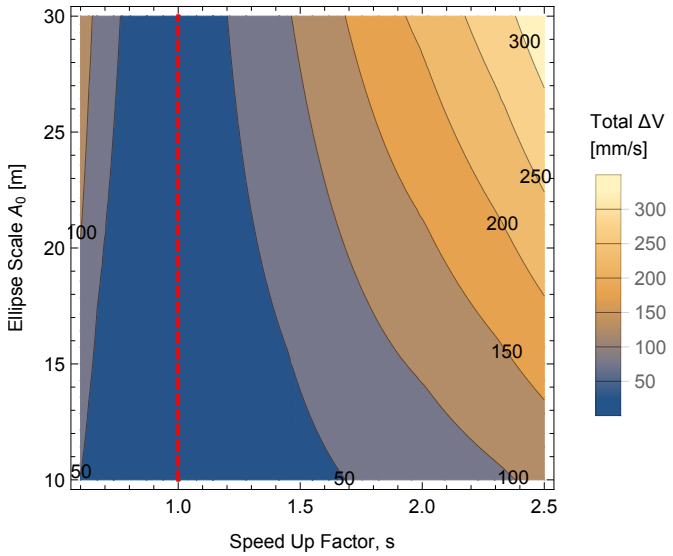

Figure 11. Total ΔV for the 2 waypoint elliptic chief. Nominal is shown by —- .

that the elliptic chief relative orbit requires greater ΔV for the same speed up factor. This is largely attributed to the nonlinear time of flight experienced by the deputy around and elliptic chief. To affect the same speed up change, a greater ΔV than the circular counterpart is required. A dramatic near singular solution exists in the implementation of the speed up factor. Not shown in Figure 11 are the ΔV contours for $s = 0.5$. In the elliptic chief case, a speed up of $s < 0.5$ constitutes a segment-wise multiple revolution solution when using the periapse and apoapse waypoints. The STM is solution is ill-equipped to address the multi-revolution solution for the elliptic chief. This is a topic of future investigation.

Presented is a selected case of the elliptic chief faster than natural circumnavigation. Demonstrated is the applicability of the proposed STM methodology to general faster than natural circumnavigation reconfigurations.

CONCLUSIONS

A methodology is presented for developing impulsive faster-than-natural circumnavigation solutions for general orbit geometries. The general relative motion state transition matrix is developed from an orbit-element difference formulation for both the circular and elliptic chief cases.Two cases are shown of circular chief faster-than-natural circumnavigation and one case of an elliptic chief. The results demonstrate how the natural planar relative orbit trajectory becomes a three-dimensional curve if the circumnavigation time is sped up or slowed down. A maximum three-dimensional warping is found to occur around a speed up factor of 2 for the circular chief case. As the speed up factor is further increased, the non-planar warping is reduced bak towards the nominal plane. Further, for the elliptic chief case, the way-point matching may result in more complex relative trajectories due to the periapse and apoapse regions. Future work will consider a greater range of elliptical chief cases and will consider eccentric anomaly, mean anomaly, and/or direct orbit element difference formulations.

REFERENCES

[1] E. Hogan and H. Schaub, "Space Debris Reorbiting Using Electrostatic Actuation," *AAS Guidance and Control Conference*, Breckenridge, CO, Feb. 3–8 2012. Paper AAS 12–016.

[2] Y. Masutani, M. Matasushita, and F. Miyazaki, "Flyaround Maneuvers on a Satellite Orbit by Impulsive Thrust Control," *Proceedings of the 2001 IEEE International Conference on Robotics & Automation*, Vol. 1, 2001, pp. 421–426, 10.1109/ROBOT.2001.932587.

[3] S. D. Straight, "Maneuver design for fast satellite circumnavigation," Master's thesis, Air Force Institute of Technologyr, March 2004.

[4] W. Zhou, J. Yuan, and J. Luo, "Flying Robots Fast Circumnavigation Trajectory Design and Guidance," *IEEE International Conference on Robotics and Biomimetics*, Dec. 2006, pp. 263–267, 10.1109/ROBIO.2006.340164.

[5] J.-j. Luo, W.-y. Zhou, and J.-p. Yuan, "A general method of trajectory design and guidance for fast satellite circumnavigation," *Journal of Astronautics*, Vol. 3, 2007, p. 023.

[6] D. P. Dannemiller, "Multi-Maneuver Clohessy-Wiltshire Targeting," *AAS/AIAA Astrodynamics Specialist Conference*, Girdwood, Alaska, July 31 – August 4 2011. Paper AAS 11-650.

[7] D.-W. Gim and K. T. Alfriend, "The State Transition Matrix of Relative Motion for the Perturbed Non-Circular Reference Orbit," *AIAA Journal of Guidance, Control, and Dynamics*, Vol. 26, No. 6, 2003, pp. 956–971.

[8] H. Schaub and J. L. Junkins, *Analytical Mechanics of Space Systems*. Reston, VA: AIAA Education Series, 2nd ed., October 2009.

[9] H. Schaub and K. T. Alfriend, "Hybrid Cartesian and Orbit Element Feedback Law for Formation Flying Spacecraft," *AIAA Journal of Guidance, Control, and Dynamics*, Vol. 25, March–April 2002, pp. 387–393.

[10] K. T. Alfriend, H. Schaub, and D.-W. Gim, "Gravitational Perturbations, Nonlinearity and Circular Orbit Assumption Effect on Formation Flying Control Strategies," *Proceedings of the Annual AAS Rocky Mountain Conference*, Breckenridge, CO, Feb. 2–6 2000, pp. 139–158.

[11] D. A. Vallado, *Fundamentals of Astrodynamics and Applications*. Microcosm Press, 4th ed., March 2013.